Theory of bonding, strain, and segregation in germanium-carbon alloys

P. C. Kelires

Physics Department, University of Crete, P.O. Box 2208, 710 03 Heraclion, Crete, Greece
and Foundation for Research and Technology-Hellas (FORTH), P.O. Box 1527, 711 10 Heraclion, Crete, Greece
(Received 27 January 1999)

We investigate the bulk and surface structure of $Ge_{1-x}C_x$ alloys using Monte Carlo simulations in the semigrand canonical ensemble, within the empirical potential formalism. We consider free-floating alloys as well as epitaxial alloys on Si and Ge substrates. The lattice constants as a function of carbon content are calculated and fitted to quadratic expressions for easy reference. Large deviations (negative bowing) from Vegard's law are found. We confirm the presence of Ge–C bonds and thus of substitutional carbon in the bulk of the material, for both epitaxial conditions. The most probable bulk carbon-carbon configurations are in a third-nearest-neighbor arrangement. The surface structure of alloys strained on Ge is characterized by strong segregation of carbon to the top layers. Segregation is less effective in alloys strained on Si. Most probable dimer configurations are both C–C and Ge–C dimers, for low carbon contents and Ge-substrate conditions, and Ge–C dimers for higher carbon contents and both epitaxial conditions. [S0163-1829(99)03839-4]

I. INTRODUCTION

Semiconductor alloys containing carbon have attracted considerable attention in recent years both because of a practical and a fundamental point of view.[1] The quest for electronic devices that are based on new semiconductor compounds demands high quality, stability, and flexibility in their design. The anticipated properties of such materials are supplementary to and even beyond those exhibited by the more traditionally used materials such as silicon. Incorporation of carbon into such traditional materials seems to open some different ways toward this direction, because it offers improved mechanical stability, manipulation of the lattice constant, and the possibility for tailored electronic properties.

It is extremely interesting from a fundamental point of view to characterize and investigate the properties of these carbon containing alloys. The greatest challenge is to deal with their *metastable* nature. In the past, they were considered as hypothetical materials because of the very small carbon solubility ($\leqslant 2\times 10^{-3}$ at. %) in the silicon, or germanium, lattice under equilibrium conditions. This is due to the large atomic size mismatch and the resulting cost in elastic energy as carbon is incorporated into the lattice. It is now possible to fabricate alloys with carbon contents well above the equilibrium solubility limit using nonequilibrium methods, such as molecular-beam epitaxy or solid phase epitaxy, which exploit the less constrained environment and the higher atomic mobility on surfaces.[2] This enhances the solubility by several orders of magnitude.[3]

The most extensively studied cases, both experimentally and theoretically, are the ternary $Si_{1-x-y}Ge_xC_y$ and binary $Si_{1-x}C_x$ alloys, usually grown on Si substrates. The former have attracted considerable attention as an alternative to the well-established and characterized binary $Si_{1-x}Ge_x/Si$ system,[4] because they have certain advantages: incorporation of carbon into the SiGe lattice can compensate the built-in compressive strain due to the lattice mismatch with the Si substrate,[5-7] and they could also manipulate the band gap and band offsets.[8-10] Research on the $Si_{1-x}C_x$ alloys is mostly motivated by the desire for band-gap manipulation. In both cases, experimental efforts aim at producing pseudomorphic layers on or in Si, which are free from extended defects and can be used in quantum well structures with strong photoluminescence signal.[11] Theoretical efforts focused on the accurate description of the lattice response upon carbon incorporation, on the surface structure, and on how the band gap is varied with carbon content. Large deviations from Vegard's law, which demands that the lattice parameters and the elastic constants adhere to a linear interpolation scheme of the elemental constants, have been predicted.[6,12,13] These are verified both experimentally[14,15] and theoretically.[7] A repulsive Ge–C interaction[6] and a preferential arrangement of C atoms[2,6] in the Si lattice are found. Surface composition profiles have been calculated and specific carbon-induced reconstructions of the (100) surface are proposed.[16-18] The band gap of the alloys seems to decrease with carbon content.[9,10] The extent of this reduction and its origins have been recently investigated.[19]

Another metastable alloy that can operate as an alternative pathway for Si-based band-gap engineering, especially at the 1.3-μm wavelength region suitable for fiber-optic systems, is the $Ge_{1-x}C_x$ compound. The solid mixture of Ge and C is very interesting. It is well known from theoretical calculations[20,6] that the zinc-blende (ZB) structure of the GeC compound is unstable toward phase separation into its segregated components at zero pressure, contrary to the very stable ZB-SiC alloy. In a sense, this fundamental difference gives an appealing advantage to nonstoichiometric $Ge_{1-x}C_x$ alloys compared to the $Si_{1-x-y}Ge_xC_y$ and $Si_{1-x}C_x$ compounds: in the latter case, both the chemical energy and the size mismatch contributions to the enthalpy of formation lead at high post-growth annealing temperatures ($\geqslant 1100$ K) to the formation of ZB-SiC precipitates.[21,22] This lowers the energy and relieves the strain. In the former case, no similar formation of bulk ZB-GeC is expected because the large chemical-energy cost overwhelms the strain relief. On the other hand, the inherent driving force for decomposition might lead to strong segregation effects, espe-

cially at the surface of the material. This issue must be investigated.

Ge$_{1-x}$C$_x$ alloys have recently been studied experimentally with respect to growth[23–25] and microstructural development,[26,27] bonding characterization,[27–29] and photoresponsivity.[30] The material is usually grown on Si or Ge substrates. Some marked differences, especially with respect to the bonding characteristics, exist between the two cases.[28,29] A theoretical investigation of the bulk and surface structure, and of the electronic structure, is lacking.

In this paper, as a first step toward the understanding of these interesting alloys, we study their fundamental bulk and surface structural properties. We apply the same theoretical methodology, utilizing atomistic Monte Carlo (MC) simulations within the empirical potential approach, used successfully before for the study of Si$_{1-x-y}$Ge$_x$C$_y$ and Si$_{1-x}$C$_x$ alloys.[6,12,13,16,17] We address various issues such as bonding characteristics (possible types of bonds for different substrate conditions), lattice constants and deviations from Vegard's law, carbon profiles, and possible dimer structures on the reconstructed (100) surface. The paper is organized as follows. In Sec. II we outline the methodology on which the MC simulations are based. The last section gives the results and the accompanying discussion, starting with the bulk properties and continuing with the surface properties.

II. METHODOLOGY

The key point in discussing the bulk and surface properties of such alloys lies in the proper incorporation of substitutional carbon atoms in the lattice. This requires the identification of the most favorable configurations involving carbon that minimize the strain. In the bulk case, these geometries are metastable, but segregation of species is rather inhibited at typical growth temperatures because diffusion is very slow. We thus describe them as being in "quasiequilibrium." In the surface problem this difficulty does not arise because the enhanced atomic mobility on and near the surface establishes instant local equilibrium in the top layers.[2,3] So, at a first level of accuracy, one considers the bulk geometries performing statistical ensemble averages over them and calculating the desired properties. At a higher level of accuracy, one identifies the most probable surface configurations, which are then assumed to be frozen in as further material is deposited on top and made inaccessible to diffusion. This process determines the final bulk structure of the epitaxial alloy film.

In both approaches, the identification of the most favorable configurations must be done in the statistically proper way. Static calculations on a limited number of configurations, generated by randomly inserting carbon atoms in the lattice, cannot arrive even at a minimum level of equilibration, because they are done at zero temperature, include only positional contributions to the free energy, and cannot capture the important aspects of the problem at growth or annealing temperatures. What we need are calculations at finite temperatures that minimize Gibb's free energy and simulate atomic diffusion so that statistical ensemble averages are taken.

One way to achieve this goal is to simulate *actual diffusion* of atoms in the network. This requires the use of molecular-dynamics (MD) simulations. The problem with this approach is that MD techniques fail to reach equilibrium in practical times because of the extremely slow diffusion in the bulk. The surface environment, which in semiconductor compounds is inhomogeneous and reconstructed, is also problematic. Here, instead of simulating actual diffusion of atoms, we make use of Ising-type flips (atom identity switches), avoiding the dynamical aspects of the problem. For alloys with relatively small atomic size mismatch, such as SiGe, this procedure is straightforward. For systems with large size mismatch, as in the present case, the flips are energetically very costly. We overcome this difficulty by using a recently introduced state-of-the-art MC algorithm[6] that enhances significantly the phase-space sampling over the metastable configurations of the alloy.

We describe for clarity the central ideas embodied in this algorithm. The underlying statistical ensemble is the *semi-grand* canonical (SGC) ensemble, denoted as $(\Delta\mu, N, P, T)$, which was used successfully before in simulations of metal alloys[31] and semiconductor alloys[32–34] with small size mismatch. This ensemble allows fluctuations in the number of atoms of each species (but keeping the total number of atoms N fixed) as a result of exchanges of particles within the system, driven by the appropriate chemical potential difference ($\Delta\mu = \mu_{Ge} - \mu_C$, in the present case). The new element in our approach is that the identity flips are coupled with appropriate relaxations of nearest-neighbor (nn) atoms, so as to lower the high barriers for diffusion in systems characterized by large atomic size mismatch and make the flips less costly. The SGC ensemble can be viewed as a special case of the grand canonical ensemble (μ, V, T) obtained by imposing the constraint that $N = \Sigma_i N_i$ is fixed and changing to constant pressure.[35] The resulting partition function (only configurational part) for an n-component mixture, which couples volume changes, atom identity flips, and displacements, is given by

$$Q_{semi} = \beta P \int dV e^{-\beta PV} \frac{V^N}{N!}$$

$$\times \sum_{identities} \prod_{i=1}^{n} \left(\frac{\lambda_i}{\lambda_1}\right)^{N_i} \int ds^N e^{-\beta U(s^N)}, \quad (1)$$

where $\lambda_i = e^{\mu_i/k_B T}$ are the fugacities in the system, $U(s^N)$ is the potential energy associated with both atom identities and displacements and is a function of the $3N$ scaled atomic coordinates s, and $i = 1$ is the arbitrarily fixed identity to which all chemical potential differences (there are $n-1$ independent fugacities in the system) are referred.

The implementation of this ensemble for MC simulations, modified to include nn relaxations, is done through the Metropolis algorithm in the following way. The change in the potential energy of the alloy at a given MC step is a sum of three terms:

$$\Delta U(s^N) = \Delta U_{displ}(s^N \to s'^N) + \Delta U_{flip}(s^N)$$

$$+ \Delta U_{relax}(s^N \to s'^N), \quad (2)$$

where s^N is symbolic for the $3N$ scaled atomic coordinates in the cell. The first term is the change due to random displacements, the second is due to identity flips, and the third is due

to the accompanying relaxations. The traditional random atomic moves ($s^N \to s'^N$) and the volume changes $V \to V'$ are accepted with a probability

$$P_{\text{acc}} = \min[1, \exp(-\beta \Delta W)] \sim e^{-\Delta W/k_B T}, \qquad (3)$$

where

$$\Delta W = \Delta U_{\text{displ}}(s^N \to s'^N) + P(V' - V) - N k_B T \ln(V'/V), \qquad (4)$$

as in the more familiar isobaric-isothermal (N, P, T) ensemble. For the trial moves that select one of the N particles at random, and with equal probability change its identity into one of the other possible identities of the system, the acceptance probability is given by

$$P_{\text{acc}}^{\text{iden}}(i \to i') = \min\left[1, \frac{\lambda_{i'}}{\lambda_i} \exp[-\beta \Delta U(s^N)]\right]$$

$$\sim e^{\beta \Delta \mu} e^{-\beta \Delta U(s^N)}. \qquad (5)$$

$\Delta U(s^N)$ denotes the change in potential energy due to the identity ($i \to i'$) flip and the accompanying relaxations, so it is the combined effect of the last two terms in Eq. (2). This can be expressed more rigorously as

$$\Delta U(s^N) = E_{\text{cluster}}\left(i \to i', \sum_{k=1}^{nn} \sum_{j=1}^{3} \Delta s_k^j(r_{0k}^j)\right) - E_{\text{cluster}}^0. \qquad (6)$$

The energy is estimated over the cluster of atoms affected by the move and the relaxations before and after the move. Each nearest neighbor is relaxed away or toward the central atom (which changes identity from i to i' and is labeled 0) in the bond direction $\vec{r}_{0k}$. In this way every scaled coordinate s^j is altered according to the scheme

$$\Delta s_k^j(r_{0k}^j) = A_{\text{bond}} r_{0k}^j, \qquad (7)$$

$$A_{\text{bond}} = \{b_{0k}[i'(0), i(k)] - |\vec{r}_{0k}|\} \chi_{\text{rel}}/|\vec{r}_{0k}|, \qquad (8)$$

where b_{0k} is the bulk equilibrium bond length among atoms 0 (after the flip) and k. In principle, one could choose b_{0k} to be the bond length associated with the specific environment at hand. For example, the value of b_{0k} could differ for bulk and surface bonds. Provided that flips are followed by a large number of random moves and volume changes, to completely relax the structures, the initial choice has no effect on the acceptance rate. The relaxation parameter χ_{rel}, ranging from 0.0 to 1.0, decides the extent of the relaxation (expressed by A_{bond}). There is a drastic increase of switch success rate, relative to null relaxation, with increasing χ_{rel}. We demonstrate this effect in Fig. 1(a) for Ge$\leftrightarrow$C flips at $T = 900$ K, appropriate for typical growth conditions. The success rate peaks at $\chi_{\text{rel}} \sim 0.7$ and eventually drops when the bond relaxes towards its ideal bulk value, due to straining of the backbonds in the neighboring atoms. Figure 1(b) shows the energy gain contributed by the cluster of atoms that are affected by the flip relaxation move as a function of χ_{rel}. A significant gain of ~ 0.4 eV/atom takes place at $\chi_{\text{rel}} \sim 0.7$, the value that maximizes the switch success rate, compared with the case when a flip is attempted but no relaxation of
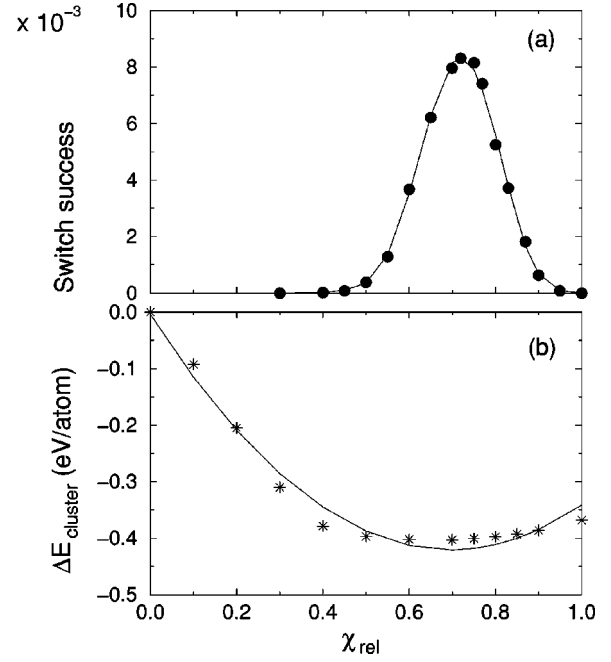
FIG. 1. Testing the effect of nn relaxations in atom identity flips at 900 K. (a) Variation of switch success rate with the relaxation parameter χ_{rel} (see text). (b) The energy of cluster of atoms affected by a flip move as a function of χ_{rel}. The zero of the energy scale corresponds to the cluster energy with null relaxation.

nearest neighbors is performed. We follow this initial procedure at every desired temperature in order to get the optimum χ_{rel} for the simulations.

For the investigation of certain properties, it is preferable to work with a fixed alloy composition. In this case we start with the SGC ensemble in order to achieve the desired compositions. We then switch to the (N, P, T) ensemble, which, however, still includes identity flips but in the form of *mutual particle interchanges* (from Ge to C at a randomly chosen site and vice versa at another site), so that the composition is kept constant. This is equivalent to removing the chemical potential terms in Eqs. (1),(5), since there is no dependence on $\Delta \mu$ any more but keeping everything else intact including the nn relaxations.

The rather complicated MC algorithm described above, with many interdependent kinds of moves, makes it prohibitively difficult at present to use energies [entering Eq. (2)] derived from *ab initio* or even tight-binding calculations. So, the interatomic interactions in the alloy in the present work are modeled within the empirical potential approach, which lacks quantum-mechanical information but allows for much greater statistical precision and the use of large cells, compensating in part the sacrifice in accuracy. We use the potentials of Tersoff for multicomponent systems,[36] which have been extensively tested and applied with success in similar contexts (Si$_{1-x-y}$Ge$_x$C$_y$ and Si$_{1-x}$C$_x$ alloys).[6,12,13,16,17] Various predictions made in these works are verified experimentally.[14,15,37] The potentials have been shown, by comparison to accurate *ab initio* calculations,[16] to describe strained configurations very well. The scheme starts with potentials for the elemental systems Ge and C. The cross interaction is derived from the elemental parameters by interpolation, using a single extra parameter. We have previously

determined this parameter[6] by fitting to the enthalpy of formation ΔH of the hypothetical ZB-GeC alloy, which was calculated to be 0.2 eV/atom and shows a strong tendency for phase separation at zero pressure.[6,20] The prediction for a repulsive Ge–C interaction in the Si lattice[6] is verified experimentally.[37]

To perform the simulations, we use supercells of various sizes and types with periodic boundary conditions. We use 512-atom cells to study the bulk properties. The cells are either cubic when simulating the ''free-floating'' alloys (the material is allowed to take its natural lattice constant) or tetragonal when simulating the epitaxial alloys, which are constrained to match the lattice constant of the substrate. For the surface studies we use (12×12)-slab supercells consisting of 16 (100) layers (in total 2304 atoms) with dimerized reconstructed surfaces. The boundary conditions are applied in either all three directions, for the bulk problem, or in the two lateral directions when treating the surface problem.

III. RESULTS AND DISCUSSION

A. Bulk properties

Lattice parameters. We first discuss the fundamental issue of how the lattice constants of the alloy vary with carbon content. It is very important to have reliable estimates of the lattice constants. Experimental work uses these values, in general, to extract the carbon contents from indirect measurements (like Rutherford backscattering, x-ray diffraction, or Raman spectroscopy). In the absence of theoretical values, it was common to utilize Vegard's law, which demands that the lattice parameters adhere to a linear interpolation scheme of the elemental constants. As mentioned in the Introduction, however, we have found in the past strong deviations from this linear rule in other carbon containing alloys,[6,12,13] leading to overestimation of the carbon content by as much as 30%. This in its turn has significant consequences on the correct description of the band-gap variation with carbon content.[19]

There are two cases to address: free-floating alloys with relaxed lattice constant a_0 and epitaxially strained alloys with the lateral lattice constant $a_{\parallel}$ matching that of the substrate, while the perpendicular lattice constant $a_{\perp}$ is free to vary. In the first case we have cubic cells, in the second case tetragonal cells. To generate the alloys, we start with pure Ge cells. The goal is to have a controlled incorporation of substitutional carbon atoms in the lattice. We choose for this the temperature of 900 K, appropriate for typical growth conditions. We then vary the chemical potential difference $\Delta \mu_{\text{Ge-C}}$, or equivalently the carbon chemical potential μ_C, to increasing values to obtain the desired carbon content. ''Guess'' values of the chemical potentials to start with are the cohesive energies per atom of the respective bulk crystal: $\mu_C = -7.37$ eV, $\mu_{\text{Ge}} = -3.85$ eV.

Most of the properties described in the present work are taken at 900 K. For the lattice constants, it is customary to present the values at 300 K. Since atom identity flips for the generation of cells are rare at such low temperatures, we use the following procedure. Five different configurations for each x at 900 K are generated using the SGC ensemble. Then we switch to the N,P,T ensemble and average over the cell dimensions for thousands of MC steps at 300 K to obtain a_0,
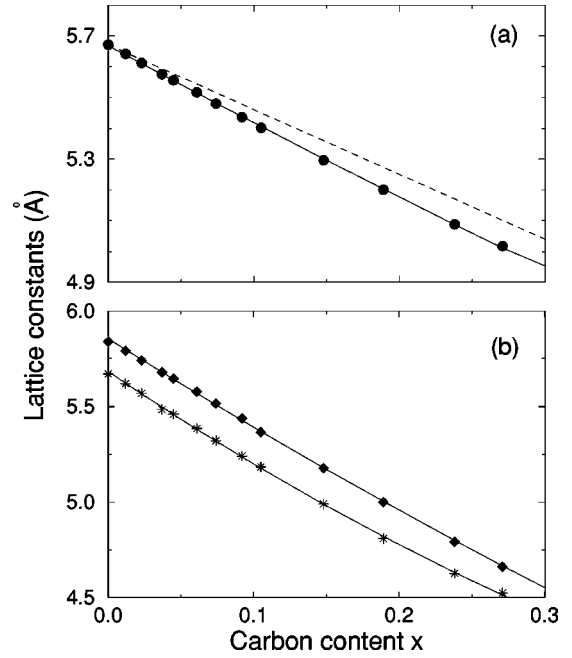
FIG. 2. Lattice constants as a function of carbon content x at 300 K. Solid lines are fits to the points. (a) Free-floating lattice constant a_0. Dashed line follows variation according to Vegard's rule. (b) Perpendicular lattice constants $a_{\perp}$ for alloys strained on Ge (stars) and alloys strained on Si (diamonds).

or $a_{\perp}$, for each configuration. Averaging over the three configurations gives a_0, or $a_{\perp}$, for each x.

The results of our calculations for the lattice constants as a function of carbon content x are given in Fig. 2. The technologically interesting cases refer to carbon contents that are limited to few percent. Here for clarity and improved statistics, and for anticipated experimental applications that might arise when epitaxial techniques progress, we extend the range of x to 0.3. Panel (a) gives the variation for the relaxed lattice constant a_0. We observe a negative deviation from Vegard's linear rule, $a_0(x) = (1-x)a_{\text{Ge}} + xa_C$, an effect observed before in $\text{Si}_{1-x-y}\text{Ge}_x\text{C}_y$ and $\text{Si}_{1-x}\text{C}_x$ alloys as well.[6,7,12,13] This effect is well known for ZB-SiC, where a negative bowing of -0.14 Å occurs, and is attributed to charge transfer from Si to C.[38] The hypothetical ZB-GeC alloy shows a similar deviation, -0.11 Å.[1] The variation of the lattice constant with x is very well fitted with the second-order polynomial

$$a_0(x) = 5.67 - 2.55x + 0.45x^2 \tag{9}$$

that reproduces the behavior at low x quite accurately. We have included in the fit the lattice constant of diamond (3.57 Å, not shown in the figure). The deviation from linear behavior is usually quantified in terms of the bowing parameter θ: a parabolic dependence of the lattice constant on concentration is incorporated by adding the term $\theta x(1-x)$ to Vegard's law,

$$a_0(x) = (1-x)a_{\text{Ge}} + xa_C + \theta x(1-x)$$

$$= a_{\text{Ge}} + (a_C - a_{\text{Ge}} + \theta)x - \theta x^2. \tag{10}$$

Comparison with Eq. (9) yields a bowing parameter $\theta = -0.45$ Å. We have found a similar large bowing of $\theta = -0.57$ Å in the case of $Si_{1-x}C_x$ alloys.[13]

More relevant to experimental work are the perpendicular lattice constants $a_\perp$ of alloys grown pseudomorphically on a given substrate. $Ge_{1-x}C_x$ alloys are usually grown on Si(100) or Ge(100) substrates. The results of our calculations for $a_\perp$ for the two cases are given in panel (b) of Fig. 2. Quadratic fits to these points give the following variations of $a_\perp$ with x. For $a_s = a_{Ge}$, we have

$$a_\perp(x) = 5.68 - 5.14x + 3.04x^2. \qquad (11)$$

For $a_s = a_{Si}$, the variation is given by

$$a_\perp(x) = 5.85 - 4.67x + 0.95x^2. \qquad (12)$$

Not included in these fits is the point for $x = 1.0$, which corresponds to diamond pseudomorphically strained on Si or Ge. This is not possible to achieve due to the large size mismatch. Equation (11) and (12) might be useful to researchers wishing to have a direct comparison with their measurements or to derive lattice data from simple formulas that can be used to extract the concentration of the alloy.

To quantify even further the nonlinear behavior of lattice parameters, we have calculated the deviations from Vegard's law and elasticity theory at the growth temperature of 900 K. For free-floating bulk alloys, we calculate the difference $\Delta a_0 = a_0^{Veg} - a_0^{MC}$, where a_0^{Veg} is the equilibrium lattice constant predicted by Vegard's rule, and a_0^{MC} is our direct MC result. For epitaxially strained alloys, we compute the difference $\Delta a_\perp = a_\perp^{MTE} - a_\perp^{MC}$. In this case the direct MC values for $a_\perp$ are compared to linearly interpolated values given by the macroscopic theory of elasticity (MTE),

$$a_\perp(x) = a_0(x)\left[1 - \frac{2c_{12}(x)}{c_{11}(x)} \times \frac{a_{substr} - a_0(x)}{a_0(x)}\right], \qquad (13)$$

with the assumption that $c_{11}(x)$ and $c_{12}(x)$, the two of the three elastic constants of the alloy, as well as $a_0(x)$, are linearly interpolated from the elemental values. The results of the calculations are given in Fig. 3. Significant deviations are found, even for such low carbon contents and at this relatively high temperature, both for the bulk alloys but most noticeably for the epitaxially strained alloys. As shown previously,[12] one can still utilize Eq. (13) and get very good agreement with the calculated $a_\perp^{MC}$ values, by using the direct values for a_0 that are easily derived from Eq. (9), instead of interpolated ones. Also, from our results it comes out that for a fully strained compensated alloy on a Si substrate one needs to incorporate $\sim 9\%$ of carbon, as can be easily checked using Eq. (12).

Microscopic bonding configurations. One of the issues of practical importance is the confirmation of the presence of substitutional carbon and its relative ratio to interstitial carbon in the Ge lattice. Related to this is the issue of the microscopic distribution of carbon atoms. A commonly used experimental probe of such properties is Raman spectrocopy. It was observed in recent studies that Raman spectra taken from $Ge_{1-x}C_x$ alloys grown on Si substrates do not reveal a Ge–C local mode,[28] which signifies the presence of substitutional C, due probably to the much stronger Si line origi-
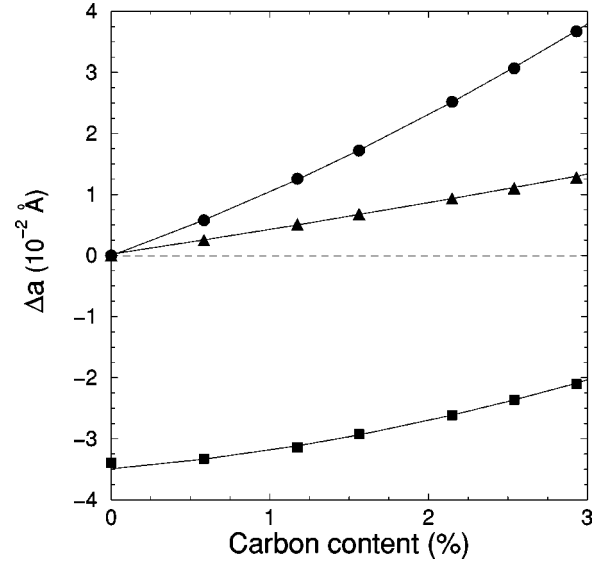
FIG. 3. Deviations of direct MC results for the lattice constants from linearly interpolated values at 900 K, as a function of carbon content. Triangles show the free-floating case (deviation from Vegard's rule). The epitaxial cases (deviations from MTE with linear a_0 and c_{ij}'s) are depicted by circles (Ge substrate) and squares (Si substrate). Solid lines are fits to the points.

nating from the c-Si substrate. Consequent work, instead, found that spectra from alloys grown on Ge substrates reveal the Ge–C mode.[29] We checked these issues by examining the pair distribution functions $g(r)$ in the alloy for both epitaxial conditions at 900 K. We concentrate at a low carbon content of 2%, appropriate for good quality thin films and at which the fraction of interstitial carbon is believed to be low. (At the moment our MC algorithm can treat only the substitutional case.) The results of this analysis are given in Fig. 4. We see from panels (a) and (b) that the C–Ge correlations are almost the same in both cases, and that the first peak representing the Ge–C bonding in the lattice is as strong when the alloy is strained on Si as when it is strained on Ge. So, we conclude that Ge–C bonds are present also in the first
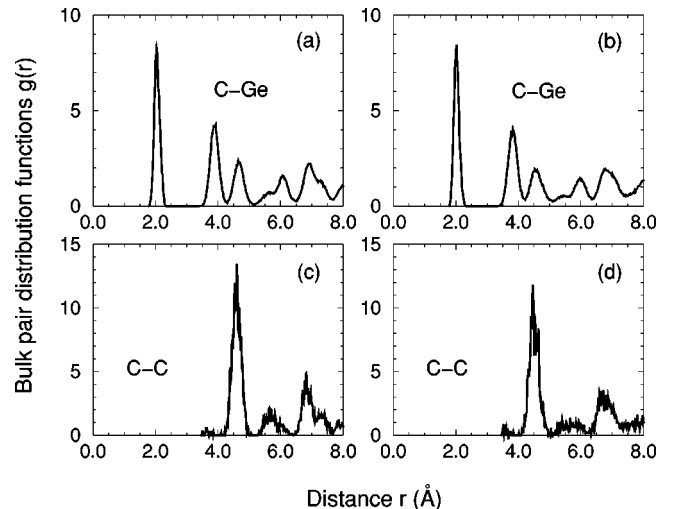
FIG. 4. Bulk partial pair distribution functions of a $Ge_{0.98}C_{0.02}$ alloy at 900 K. In panels (a) and (c) the alloy is strained on Ge. In panels (b) and (d) the alloy is strained on Si.

case, but they are not observed in the Raman spectra due to the obstruction from the Si substrate. The average bond length at 900 K is 2.05 Å. The situation is drastically different in $Si_{1-x-y}Ge_xC_y$ alloys where Ge–C bonds in the Si lattice are energetically unfavorable compared to Si–C bonds.[6]

Panels (c) and (d) of Fig. 4 display the C–C correlations in the Ge lattice. Again, we see a similarity in the correlations for both epitaxial conditions, with the peaks a little stronger when the alloy is strained on Ge. Most importantly, we observe the same trends as in $Si_{1-x-y}Ge_xC_y$ (Refs. 6 and 12) and $Si_{1-x}C_x$ alloys,[2] namely, an oscillatory C–C correlation with a very repulsive interaction at short distances. This is marked by the absence of the first- and second-nn peaks (as well as of the fifth and eighth peak) and a strong enhancement of the third-nn peak. Thus, there is a preferential arrangement of C atoms as third $nn's$, a configuration that minimizes the elastic (strain) energy in the lattice.

B. Surface properties

We now proceed to investigate the surface structure and properties of $Ge_{1-x}C_x$ alloys. There are some marked differences with the bulk case.

Surface composition profile. As we discussed in the Introduction, formation of the bulk ZB-GeC phase in $Ge_{1-x}C_x$ alloys is not possible, because the large chemical-energy cost to form this structure overwhelms the resulting strain relief. The surface factor with the much less constrained environment and the lower diffusion barriers offers another possibility. The lattice elastic energy due to the atomic size mismatch, which is appreciable even in the more frequently occurring third-nn configurations, could be relieved through segregation of carbon atoms at the surface region. Low-energy surface structures might as well contribute to this mechanism. We investigated the segregation problem by minimizing the Gibb's free energy at a growth temperature of 900 K, using the SGC ensemble, and identifying the most probable geometries. For this study we use the 2304-atom slab supercells with dimerized reconstructed surfaces.

Let us first examine the probability distributions $P(z)$ for finding the C atoms at a certain distance z from the surface. These are shown in Fig. 5 for two low-carbon-content alloys and for both epitaxial conditions. The zero of the depth scale is at the middle of the slab, and the distance is measured from this origin as we move toward the two surfaces of the slab. There are eight layers in each direction. The peaks centered at each layer are broadened due to thermal vibrations. There are some prominent characteristics in these two profiles. In both cases there is a strong enhancement of the surface layers with carbon and a depletion of inner bulklike layers. The extent of this enhancement and the distribution of carbon, however, differ from case to case.

In panel (a), where the average alloy is $Ge_{0.974}C_{0.026}$ and is strained on Ge, we observe a strong enhancement of the top surface layer, indicating a low surface energy for C, a near depletion of the second layer (it appears only as a shoulder in the tail of the first peak), again enhancement of the third layer (but not as much as in the top layer), and a reduction in layer four. Thus we have an oscillatory behavior similar to what has been observed in $Si_{1-x-y}Ge_xC_y$ (Ref. 17) and
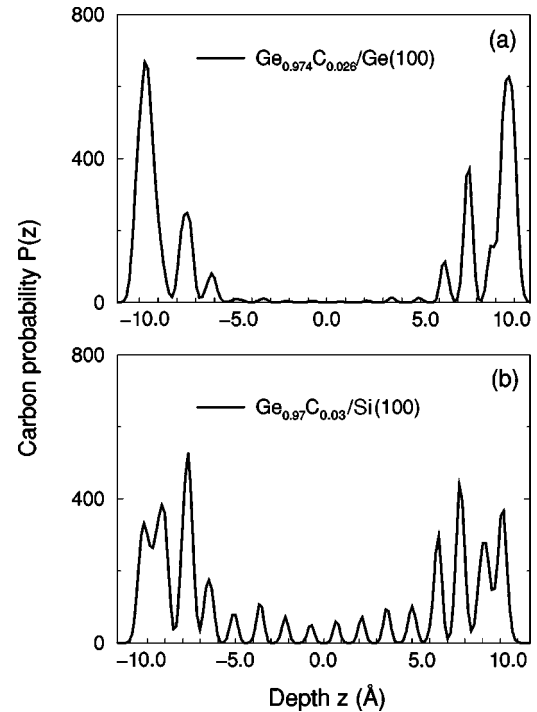
FIG. 5. Carbon probability distributions as a function of depth in slab cells (a) strained on Ge and (b) strained on Si. The zero of the depth scale is at the middle of the slabs.

$Si_{1-x}C_x$ alloys (Ref. 16) that can be explained on the basis of the repulsive interaction between nn C atoms, which prevents them from equally populating adjacent layers. The layers close to the center of the slab are almost depleted from carbon.

In panel (b) the average alloy is $Ge_{0.97}C_{0.03}$ and is strained on Si. In this case, as a general argument, we could say that segregation to the surface layers is not so effective as in the above case. The inner layers still possess an appreciable amount of carbon atoms. This behavior can be understood considering that the Ge layers on a Si substrate are under compressive stress and carbon serves to compensate this stress. The degree of segregation is therefore determined by the competition between the need of Ge–C geometries in the bulk to compensate the epitaxial strain and the attraction of carbon to certain energetically favorable sites in the subsurface layers. The top layer is much less favored, while carbon occupancy is rising in the second layer. Also, significantly enhanced are the occupancies in the third and fourth layers.

The work of Kelires and Tersoff can explain these findings.[32] The surface reconstruction induces large stresses in the subsurface layers. The second layer is under a large compression ($\simeq 0.4$ eV/atom) and tends to be occupied by the smaller atom, carbon. This effect is stronger here than in the case of a Ge substrate, because the C geometries on the top layer are less numerous and the repulsion with second layer C atoms is diminished. The overall reduction of top layer occupancy also works for the enhancement in layers three and four. The energetically favorable sites in these two layers are determined by the surface reconstruction as well. There are sites located below the surface dimers that are under compressive stress, and so favorable for carbon, and sites located between the surface dimers that are under tensile stress, and so unfavorable for carbon. Indeed, an analysis
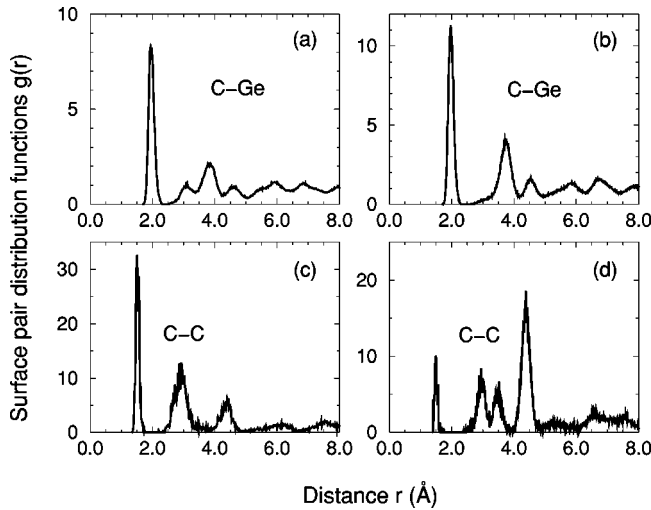
FIG. 6. Surface partial pair distribution functions of a $Ge_{0.977}C_{0.023}$ alloy at 900 K. In panels (a) and (c) the alloy is strained on Ge. In panels (b) and (d) the alloy is strained on Si.

FIG. 7. Schematic of the average distribution of dimers on the reconstructed surface of a $Ge_{0.977}C_{0.023}$ alloy strained on Ge at 900 K (ideal positions). Large empty circles denote Ge atoms. Small filled circles are C atoms. A configuration with (2×2) periodicity is enclosed in a frame.

of the average site occupancies reveals that this effect is very strong at layer three, and somewhat weaker at layer four. For alloys with a higher carbon content and thus with richer surface layers, this picture is altered, because the repulsive *nn* C–C interaction forces the occupancy of the unfavorable sites to rise.[16,17]

These conclusions are further substantiated and elaborated by examining the surface pair distribution functions of two alloys with the same composition ($Ge_{0.977}C_{0.023}$) at 900 K, shown in Fig. 6. The correlations for the alloy strained on Ge are plotted in panels (a) and (c), and those for the alloy strained on Si are plotted in panels (b) and (d). Comparing the C–Ge correlations first, we observe a weakening of all peaks when the alloy is strained on Ge. Integration of the first peak gives an average number of neighbors equal to only 2.7, compared to 3.7 for a Si substrate. This confirms that segregation has left little carbon in the inner layers, but also suggests that in the surface layers there is a smaller tendency for C to bond with Ge and an increased tendency to bond with other carbon atoms. We shall discuss this below. The average Ge–C bond length is 1.98 Å, shorter than the bulk bond length (2.05 Å), reflecting the contribution from the Ge–C dimers on the top layer. Note also that in panel (a) there is an extra peak at ~ 3.1 Å, between the first and second peak at ~ 3.7 Å, which is absent from panel (b). This C–Ge peak arises from geometries of the type C–C–Ge, where a Ge is attached to a C–C bond, most likely a C–C dimer on the top layer. The genuine second bulklike peak at ~ 3.7 Å arises from geometries of the type C–Ge–Ge.

Looking at the C–C correlations, we see further differences between the two substrate conditions but also between surface and bulk behavior. The most prominent characteristic is evident in panel (c), with the alloy strained on Ge. The third peak, the main bulk-type C–C interaction, is drastically weakened in favor of the second and, especially, the first peak, which are completely absent in the bulk. The first peak at 1.5 Å, indicates significant C–C bonding, which we anticipate to be C–C dimers on the top layer (explaining the extra C–Ge peak at ~ 3.1 Å). The second peak at ~ 3.0 Å, arises from geometries of the type C–Ge–C, involving a C
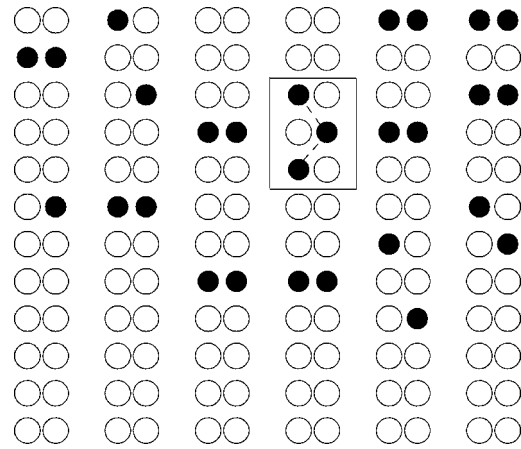
atom on the top layer, a Ge atom below in the second, and a C atom in the third layer. On the other hand, the C–C correlations in panel (d), the alloy is strained on Si, show much less C–C dimer bonding (very weak first peak) and more bulklike third-*nn* arrangements (enhanced third peak). Interestingly, we see a split second peak at ~ 3.0 Å, and ~ 3.5 Å. The first of these features arises from configurations of the type C–Ge–C as above, and the second from configurations involving a C–Ge dimer (~ 1.95 Å) on the first layer and a C atom below in the second (this layer is rich in carbon in the Si-substrate case).

Dimer configurations. Finally, we investigate in more detail the surface structure by examining the distribution of species on the top layer and identifying the types and the proportions of the formed dimers. This analysis is quantified by calculating the average site occupancies at the reconstructed surfaces that determine whether a specific site would be Ge or C. The equilibration of the composition is done with the SGC ensemble. The instantaneous identity of each site changes many times during equilibration. At the end of the run the average identity is determined. Figure 7 shows the resulting most probable dimer configurations at 900 K, on one of the two surface layers, of a slab cell representing an average alloy $Ge_{0.977}C_{0.023}$ strained on Ge. This is the case with carbon-enriched top layers (the average layer content is $\sim 20\%$ compared to the average slab content of 2.3%). Besides the Ge–Ge dimers, the majority-type dimers, we find that carbon forms both Ge–C and C–C dimers. Interestingly, the relative ratio of C–C dimers to Ge–C dimers is very high. On this surface there are nine C–C dimers and ten Ge–C dimers. On the average, taking statistics on the second surface layer of the slab as well, the ratio is $\frac{7}{10}$. Note that when Ge–C dimers approach each other they form configurations with (2×2) periodicity, which aligns the dimers in opposite directions reducing the surface stress.

The surface layers of the alloys strained on Si show a different picture. Besides the overall reduction of carbon content [see Fig. 5(b)], there is a reduction in the relative ratio of C–C dimers to Ge–C dimers. The alloy $Ge_{0.97}C_{0.03}$ has an average top layer carbon content of $\sim 11\%$, compared

to the average slab content of 3%, and a ratio of $\frac{4}{10}$. The ratio is even more reduced with increasing average carbon content in the slab. So for x larger than ~ 0.05, the ratio falls to $\frac{2}{10}$, no matter what the substrate condition is. The explanation for the overall ratio variations lies in strain energy *versus* chemical-energy considerations. We have found previously[17] that C–C dimers on the surface of $Si_{1-x-y}Ge_xC_y$ alloys strained on Si are nearly absent, despite being the strongest chemical bonds, because their formation requires large atomic relaxations in the neighborhood and induces considerable strain. Instead, Si–C dimers are favored because they induce less strain. In general, we can say that C–C dimers are acceptable only under conditions that provide a significant relief of surface stress, and when the gain in chemical energy overwhelms the strain-energy cost. In our case, for low carbon contents, this mechanism works for Ge-substrate conditions since the surface region is nearly strain free, and the C–C dimer bond is much stronger than the Ge–C dimer bond. It does not work so effectively for Si-substrate conditions because the surface region is already under considerable epitaxial strain (the Ge layers are tetragonally deformed), and formation of structures inducing further strain is not likely. Note that the necessary relaxations to accommodate a dimer involve not only atoms on the top layer but also atoms in the subsurface layers. When the carbon content on the surface layer rises, the formation of an excessive number of C–C dimers costs more in strain energy than gain in chemical energy, and the Ge–C dimers are then favored.

[1] P.C. Kelires, Int. J. Mod. Phys. C **9**, 357 (1998).

[2] H. Rücker, M. Methfessel, E. Bugiel, and H.J. Osten, Phys. Rev. Lett. **72**, 3578 (1994).

[3] J. Tersoff, Phys. Rev. Lett. **74**, 5080 (1995).

[4] See *Properties of Strained and Relaxed Silicon Germanium*, edited by E. Kasper (INSPEC, London, 1995).

[5] K. Eberl, S.S. Iyer, S. Zollner, J.C. Tsang, and F.K. LeGoues, Appl. Phys. Lett. **60**, 3033 (1992).

[6] P.C. Kelires, Phys. Rev. Lett. **75**, 1114 (1995).

[7] W. Windl, O.F. Sankey, and J. Menéndez, Phys. Rev. B **57**, 2431 (1998).

[8] R.A. Soref, J. Appl. Phys. **70**, 2470 (1991).

[9] A.A. Demkov and O.F. Sankey, Phys. Rev. B **48**, 2207 (1993).

[10] O.G. Schmidt and K. Eberl, Phys. Rev. Lett. **80**, 3396 (1998).

[11] K. Brunner, K. Eberl, and W. Winter, Phys. Rev. Lett. **76**, 303 (1996); K. Brunner, W. Winter, and K. Eberl, Appl. Phys. Lett. **69**, 1279 (1996).

[12] P.C. Kelires, Appl. Surf. Sci. **102**, 12 (1996).

[13] P.C. Kelires, Phys. Rev. B **55**, 8784 (1997).

[14] M. Meléndez-Lira, J. Menéndez, W. Windl, O.F. Sankey, G.S. Spencer, S. Sego, R.B. Culbertson, A.E. Bair, and T.L. Alford, Phys. Rev. B **54**, 12 866 (1996).

[15] M. Berti, D. De Salvador, A.V. Drigo, F. Romanato, J. Stangl, S. Zerlauth, F. Schaffler, and G. Bauer, Appl. Phys. Lett. **72**, 13 (1998).

[16] P.C. Kelires and E. Kaxiras, Phys. Rev. Lett. **78**, 3479 (1997).

[17] P.C. Kelires, Surf. Sci. Lett. **418**, 62 (1998).

[18] O. Leifeld, D. Grützmacher, B. Müller, K. Kern, E. Kaxiras, and P.C. Kelires, Phys. Rev. Lett. **82**, 972 (1999).

[19] G. Theodorou, G. Tsegas, P.C. Kelires, and E. Kaxiras, Phys. Rev. B (to be published).

[20] O.F. Sankey, A.A. Demkov, W.T. Petuskey, and P.F. McMillan, Modell. Simul. Mater. Sci. Eng. **1**, 741 (1993).

[21] G.G. Fischer, P. Zaumseil, E. Bugiel, and H.J. Osten, J. Appl. Phys. **77**, 1934 (1995).

[22] P. Warren, J. Mi, F. Overney, and M. Dutoit, J. Cryst. Growth **157**, 414 (1995).

[23] H.J. Osten, E. Bugiel, and P. Zaumseil, J. Cryst. Growth **142**, 322 (1994).

[24] J. Kolodzey, P.A. O'Neil, S. Zhang, B.A. Orner, K. Roe, K.M. Unruh, C.P. Swann, M.M. Waite, and S.I. Shah, Appl. Phys. Lett. **67**, 1865 (1995).

[25] M. Todd, J. Kouvetakis, and D.J. Smith, Appl. Phys. Lett. **68**, 2407 (1996).

[26] M. Krishnamurthy, J.S. Drucker, and A. Challa, J. Appl. Phys. **78**, 7070 (1995).

[27] M. Krishnamurthy, B.-K. Yang, and W.H. Weber, Appl. Phys. Lett. **69**, 2572 (1996).

[28] B.-K. Yang, M. Krishnamurthy, and W.H. Weber, J. Appl. Phys. **82**, 3287 (1997).

[29] W.H. Weber, B.-K. Yang, and M. Krishnamurthy, Appl. Phys. Lett. **73**, 626 (1998).

[30] X. Shao, S.L. Rommel, B.A. Orner, H. Feng, M.W. Dashiell, R.T. Troeger, J. Kolodzey, P.R. Berger, and T. Laursen, Appl. Phys. Lett. **72**, 1860 (1998).

[31] S.M. Foiles, Phys. Rev. B **32**, 7685 (1985).

[32] P.C. Kelires and J. Tersoff, Phys. Rev. Lett. **63**, 1164 (1989).

[33] B. Dünweg and D.P. Landau, Phys. Rev. B **48**, 14 182 (1993); M. Laradji, D.P. Landau, and B. Dünweg, *ibid.* **51**, 4894 (1995).

[34] A. Silverman, A. Zunger, R. Kalish, and J. Adler, J. Phys.: Condens. Matter **7**, 1167 (1995).

[35] See D. Frenkel, in *Computer Simulations in Materials Science: Applied Sciences*, Vol. 205 of *NATO Advanced Study Institute, Series E: Applied Sciences*, edited by M. Mayer and V. Pontikis (Kluwer Academic, Dordrecht, 1991), p. 85.

[36] J. Tersoff, Phys. Rev. B **39**, 5566 (1989).

[37] H. Jacobson, J. Xiang, N. Herbots, S. Whaley, P. Ye, and S. Hearne, J. Appl. Phys. **81**, 3081 (1997).

[38] J.L. Martins and A. Zunger, Phys. Rev. Lett. **56**, 1400 (1986).